On the Nonlinear Elastodynamics of Skeletal Muscle

PhD Thesis Defence | Mathematics
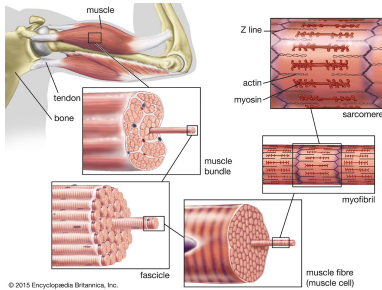
Javier A. Almonacid Paredes
Supervisor: Nilima Nigam (Mathematics)
Co-supervisor: James Wakeling (Biomedical Physiology and Kinesiology)

Motivation: 3D Dynamic Deformation of Skeletal Muscle

Muscle deformation: a multiscale phenomenon (§1.1)

Figure 1: Scales involved in the dynamics of skeletal muscle.

- Muscles can simultaneously generate **active** and **passive** force.
- Muscles generate **active** force primarily at the **sarcomere** level (~ 2 μm). Fibrous proteins in their interior slide past each other forming cross-bridges[1].
- Sarcomeres are part of a much larger structure: **the muscle fibre**, which is usually considered the fundamental unit of muscle tissue.
- We are interested in the **macroscopic** behaviour of the muscle-tendon unit, which is in the scale of mm or cm.

---

[1] J Hanson & HE Huxley (1953), AF Huxley & R Niedergerke (1954).

Hill-type models of muscle in 3D (§1.4)

- In 1D, a single fibre generates a force that depends on its stretch λ and strain rate $\dot{\varepsilon} := \frac{d\lambda}{dt} \implies$ PK1 should depend on displacement and velocity, i.e.

$$\mathbf{P} = \mathbf{P}(\lambda, \dot{\varepsilon}) = \mathbf{P}(\mathbf{U}, \mathbf{V}).$$

- However, 3D models typically solve:
  1. Quasi-static, no velocity: $\mathbf{0} = \mathbf{Div}\,\mathbf{P}(\mathbf{U})$ (Blemker 2004, Rahemi 2015, Dominguez 2020, Wakeling et al. 2020, Konno 2024).
  2. Quasi-static, variable velocity: $\mathbf{0} = \mathbf{Div}\,\mathbf{P}(\mathbf{U}; \mathbf{V})$ (Di Salvo & Blemker 2024).
  3. Dynamic, isokinetic: $\rho_0 \mathbf{U}_{tt} = \mathbf{Div}\,\mathbf{P}(\mathbf{U}; \mathbf{V})$, $\mathbf{V} = \text{constant}$ (Dominguez 2020, Ross et al. 2021, Tam 2024).

Main goal

Our main goal is to systematically develop a framework to study:

$$\rho_0 \mathbf{U}_{tt} = \mathbf{Div}\,\mathbf{P}(\mathbf{U}, \mathbf{V}), \quad \rho_0 \approx 1060 \text{ kg/m}^3,$$

in **one** and **three** dimensions, based on:

1. realistic physiology,
2. sound mathematical and numerical analysis principles,
3. a structured approach to scientific software development.

Main contributions

Ch. 2 Mass (inertial) effects can be significant for **larger muscles**, **fast dynamics**, and depend on the number of masses in a multibody model (MM).

Ch. 3 MMs are inherently dynamically unstable. A 1D continuum model reveals convexification alternatives.

Ch. 4 First-order time stepping schemes are more robust than Newmark-type schemes for velocity computations in muscle-like materials.

Main contributions (cont.)

Ch. 5 A new spatio-temporal discretization for 3D **dynamic** skeletal muscle deformation is proposed, resulting in a robust algorithm **active** musculoskeletal (MSK) simulations.

Ch. 6 A new open-source library is developed: **Flexodeal**. Dynamic, active MSK simulations show the impact of mass and nonconvexity in several contexts.

Ch. 7 Thanks to Flexodeal, **muscle gearing** can be studied for the **first time** using a continuum mechanics model.

Insights from 1D Models

Muscle force according to Hill's model (§2.2)

$$F_{Hill}(\lambda_M, \dot{\varepsilon}_M) = F_0 \left\{ \underbrace{a(t)\widehat{F}_A(\lambda_M)\widehat{F}_V(\dot{\varepsilon}_M)}_{\text{active force}} + \underbrace{\widehat{F}_P(\lambda_M)}_{\text{passive force}} \right\}$$
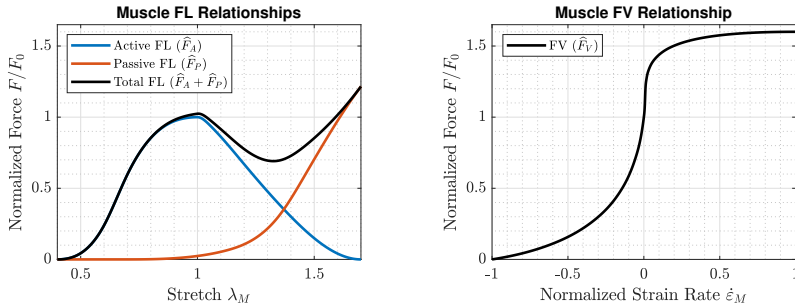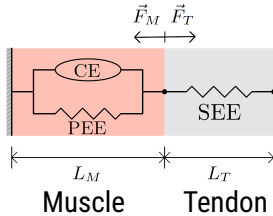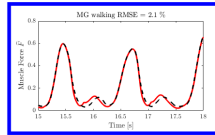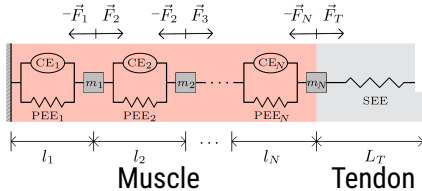

Figure 2: Force-length (FL) and force-velocity (FV) relationships in Hill's muscle model.
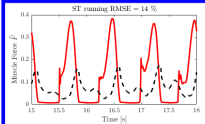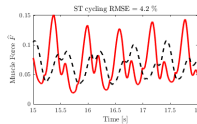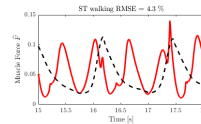
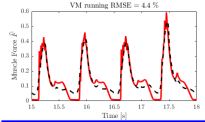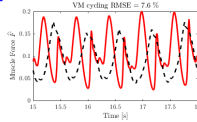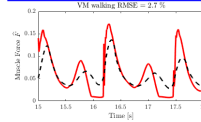# Mass effects in a 1D multibody model (§2.5)

Massless model: $F_M := F_{Hill}$

Mass-enhanced model: $F_i := F_{Hill}$

Figure 3: Predicted muscle forces (scale $s = 10$, $N = 64$ masses) for different muscle-task combinations. Model inputs obtained from a human locomotion experiment by Chen (2024).

Dynamic stability along the descending limb (Ch. 3)
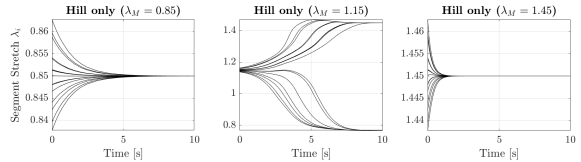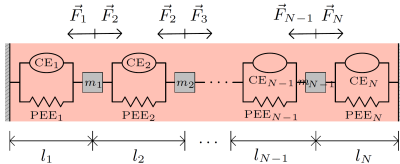
Continuum limit of MMs as $N \to \infty$: $\boxed{\rho_{0,L} u_{tt} = \left(F_{Hill}(\lambda, \dot{\varepsilon}) \right)_x}$
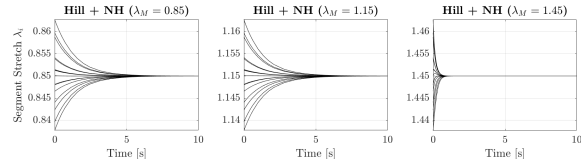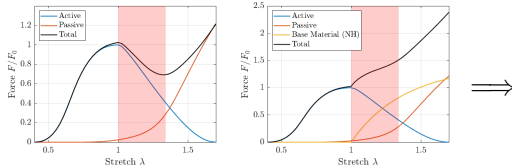
Shaded region: descending limb

$$\boxed{\rho_{0,L} u_{tt} = \left(F_{Hill}(\lambda, \dot{\varepsilon}) + \textcolor{blue}{F_{Neo-Hookean}(\lambda)} \right)_x}$$

A 3D Lagrangian Formulation

A fully dynamic 3D continuum model (§5.4)

Lagrangian formulation

Find a displacement **U**, a velocity **V**, a pressure p, and a dilatation D such that:

$$\frac{\partial \mathbf{U}}{\partial t} = \mathbf{V}, \quad \rho_0 \frac{\partial \mathbf{V}}{\partial t} = \mathbf{Div}\,\mathbf{P}(\mathbf{U}, \mathbf{V}, p, D) \quad \text{in } \mathcal{B}_0,$$

$$J(\mathbf{U}) - D = 0, \quad p - \Psi'_{vol}(D) = 0 \quad \text{in } \mathcal{B}_0,$$

$$\mathbf{U} = \mathbf{U}_D \quad \text{on } \Gamma_{D,0}, \quad \mathbf{P}(\mathbf{U}, \mathbf{V}, p, D)\mathbf{N} = \mathbf{0} \quad \text{on } \Gamma_{N,0},$$

$$\mathbf{U} = \mathbf{U}_0, \quad \mathbf{V} = \mathbf{V}_0, \quad p = p_0, \quad D = D_0 \quad \text{in } \mathcal{B}_0 \times \{t = 0\}.$$

- Model based on the 3-field formulation by Simo, Taylor, and Pister (1985).
- Using simple finite element spaces does not lead to locking, even when $J := \det(\mathbf{F}) \approx 1$. The latter is the case for skeletal muscle (Baskin & Paolini 1967).

Stress tensors (§5.1-5.3)

- We consider a volumetric/isochoric decomposition[2] of the strain-energy function, i.e.
  $\Psi = \Psi_{vol}(J) + \Psi_{iso}(\mathbf{U}, \mathbf{V})$.

- First Piola-Kirchhoff tensor (PK1): $\mathbf{P} = \mathbf{FS} = \dfrac{\partial \Psi}{\partial \mathbf{F}}$.

- Second Piola-Kirchhoff tensor (PK2):

$$\mathbf{S} = \mathbf{S}_{vol} + \mathbf{S}_{iso} = pJ\mathbf{C}^{-1} + J^{-2/3} \left(\mathbb{I} - \frac{1}{3}\mathbf{C}^{-1} \otimes \mathbf{C} \right) : \left(\bar{\mathbf{S}}_{base} + \bar{\mathbf{S}}_{fibre} \right),$$

- $\bar{\mathbf{S}}_{base} = \bar{\mathbf{S}}_{base}(\mathbf{U})$, the base material component, is usually a combination of **hyperelastic materials** describing components such as intramuscular fat (Rahemi et al. 2015) and extracellular matrix (Konno et al. 2021).

---

[2]Flory 1961, Simo & Taylor 1991.

Along-fibre stress: Hill's model (§5.2.1)

■ Let λ and $\dot{\varepsilon} := \dot{\lambda}$ denote the fibre stretch and strain rate, respectively. According to the volumetric/isochoric decomposition, their modified versions are given by:
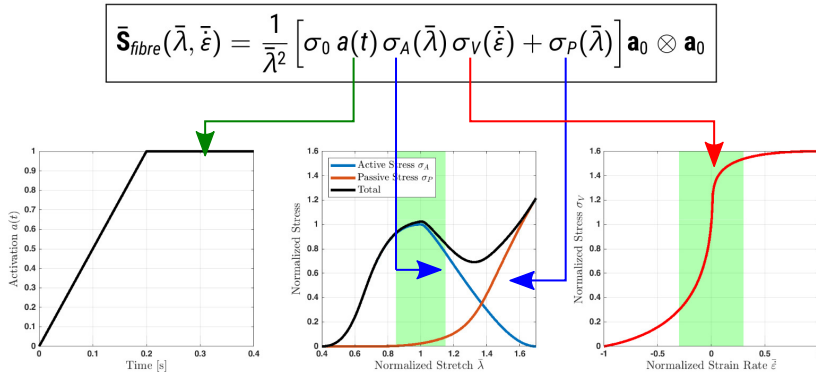
$$\bar{\lambda} = \|\bar{\mathbf{F}}\mathbf{a}_0\|, \quad \bar{\dot{\varepsilon}} = \frac{d\bar{\lambda}}{dt} = \frac{(\bar{\mathbf{F}}\mathbf{a}_0)^\top[\mathbb{P} : (\dot{\bar{\mathbf{F}}}\bar{\mathbf{F}}^{-1})^{\mathrm{sym}}](\bar{\mathbf{F}}\mathbf{a}_0)}{\bar{\lambda}}.$$

■ Then, we consider (Wakeling et al. 2020):

$$\boxed{\bar{\mathbf{S}}_{fibre}(\bar{\lambda}, \bar{\dot{\varepsilon}}) = \frac{1}{\bar{\lambda}^2} \underbrace{\sigma_0 \left[a(t)\, \sigma_A(\bar{\lambda})\, \sigma_V(\bar{\dot{\varepsilon}}) + \sigma_P(\bar{\lambda}) \right]}_{\text{Hill's model}} \mathbf{a}_0 \otimes \mathbf{a}_0.}$$

$\sigma_0 \approx 200$ kPa is the maximum isometric stress of muscle, $a(t) \in [0, 1]$ is the fibre activation, $\mathbf{a}_0$ describes the (local) initial fibre orientation. Furthermore, (σ_A, σ_P) and σ_V are derived from force-length and force-velocity relationships.

Stress-stretch and stress−strain-rate relationships

$$\bar{\mathbf{S}}_{fibre}(\bar{\lambda}, \bar{\dot{\varepsilon}}) = \frac{1}{\bar{\lambda}^2}\left[\sigma_0\, a(t)\, \sigma_A(\bar{\lambda})\, \sigma_V(\bar{\dot{\varepsilon}}) + \sigma_P(\bar{\lambda})\right]\mathbf{a}_0 \otimes \mathbf{a}_0$$

Figure 4: Functions that define the along-fibre stress. Green regions correspond to the operating range of muscles.

Time discretization (§5.5)

We choose a **fully-implicit**[3], **first-order** discretization:

$$\frac{\mathbf{U}^{n+1} - \mathbf{U}^n}{\Delta t} = \mathbf{V}^{n+1} \qquad \text{in } \mathcal{B}_0,$$

$$\rho_0 \frac{\mathbf{V}^{n+1} - \mathbf{V}^n}{\Delta t} - \mathbf{Div}\,\mathbf{P}(\mathbf{U}^{n+1}, \mathbf{V}^{n+1}, p^{n+1}, D^{n+1}) = \mathbf{0} \qquad \text{in } \mathcal{B}_0,$$

$$J(\mathbf{U}^{n+1}) - D^{n+1} = 0 \qquad \text{in } \mathcal{B}_0,$$

$$p^{n+1} - \Psi'_{vol}(D^{n+1}) = 0 \qquad \text{in } \mathcal{B}_0,$$

$$\mathbf{U}^{n+1} = \mathbf{U}_D(\cdot, t_{n+1}) \qquad \text{on } \Gamma_{D,0},$$

$$\mathbf{P}(\mathbf{U}^{n+1}, \mathbf{V}^{n+1}, p^{n+1}, D^{n+1})\mathbf{N} = \mathbf{0} \qquad \text{on } \Gamma_{N,0}.$$

---

[3] This is a departure from the semi-implicit considered by Ross et al. 2021 (see also Dominguez 2020).
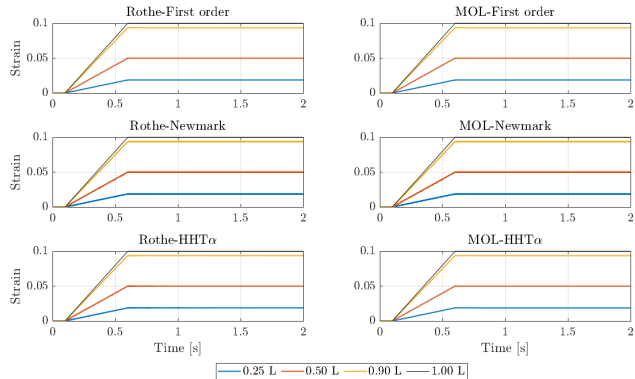
Testing different time-stepping schemes (Ch. 4)

- Three time discretizations:
  1. First-order (first row),
  2. Newmark average acceleration (middle row),
  3. HHT-α (last row).

- Two alternatives:
  1. Rothe's method (left column),
  2. MOL (right column).

- Experiment: stretch a Neo-Hookean rod to $1.1 \times L_0$. Piecewise-linear boundary condition.

Figure 5: **Strain** at three different points in the rod ($\kappa = 10^6$ Pa, $\rho_0 = 1060 \, \text{kg/m}^3$, $\nu = 0.4$, $\Delta t = 0.001 \, \text{s}$).

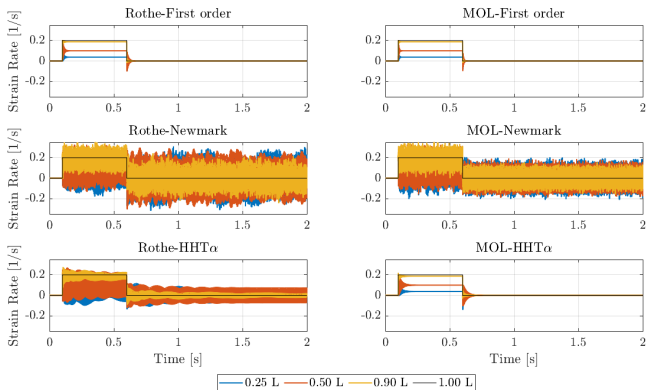# A first-order scheme can reduce spurious velocity oscillations (Ch. 4)

Figure 6: **Strain rates** for the same experiment.

Nonlinear weak formulation (§5.5)

Find $(\mathbf{U}^{n+1}, p^{n+1}, D^{n+1}) \in \mathbf{H}^1(\mathcal{B}_0) \times L^2(\mathcal{B}_0) \times L^2(\mathcal{B}_0)$ s.t. $\mathbf{U}^{n+1} = \mathbf{U}_D(\cdot, t_{n+1})$ on $\Gamma_{D,0}$ and

$$R(\mathbf{U}^{n+1}, p^{n+1}, D^{n+1}; \delta\mathbf{U}, \delta p, \delta D) =$$
$$\Delta t^{-2}\rho_0 \int_{\mathcal{B}_0} \mathbf{u}^{n+1} \cdot \delta\mathbf{U} - \Delta t^{-1}\rho_0 \int_{\mathcal{B}_0} \mathbf{V}^n \cdot \delta\mathbf{U} - \Delta t^{-2} \int_{\mathcal{B}_0} \mathbf{U}^n \cdot \delta\mathbf{U}$$
$$+ \int_{\mathcal{B}_0} \mathbf{P}^{n+1} : \nabla_0 \delta\mathbf{U} + \int_{\mathcal{B}_0} [J(\mathbf{U}^{n+1}) - D^{n+1}] \delta p + \int_{\mathcal{B}_0} [\Psi'_{vol}(D^{n+1}) - p^{n+1}] \delta D,$$

for any $(\delta\mathbf{U}, \delta p, \delta D) \in \mathbf{H}_0^1(\mathcal{B}_0) \times L^2(\mathcal{B}_0) \times L^2(\mathcal{B}_0)$. The triple $(\mathbf{U}^{n+1}, p^{n+1}, D^{n+1})$ is approximated by the finite element $\mathbf{Q}_{k+1} \times P_k \times P_k$, $k \geq 1$ (Brink & Stein, 1996).

On Polyconvexity and Convergence

Existence of energy minimizers (§5.8)

- Existence of minimizers is ensured whenever the strain-energy function of the system $\Psi(\mathbf{C}) = W(\mathbf{F})$ is **polyconvex** (Ball, 1976), that is, there exists a function $\Sigma : \mathbb{R}^{3 \times 3} \times \mathbb{R}^{3 \times 3} \times \mathbb{R}$ (in general non-unique) such that

$$W(\mathbf{F}) = \Sigma(\mathbf{F}, \operatorname{Adj} \mathbf{F}, \operatorname{Cof} \mathbf{F})$$

  is strictly convex in all its 19 components (here $\mathbf{F}$ is the deformation tensor).

- Furthermore, polyconvexity $\Rightarrow$ ellipticity (Schröder & Neff, 2003).

- The elastic free energy $W(\mathbf{F}) = \Psi(\mathbf{C})$ is **elliptic** if and only if the Legendre-Hadamard condition:

$$D_{\mathbf{F}}^2 W(\mathbf{F}).(\boldsymbol{\xi} \otimes \boldsymbol{\eta}, \boldsymbol{\xi} \otimes \boldsymbol{\eta}) \geq 0,$$

  holds for any $\mathbf{F} \in \mathbb{R}^{3 \times 3}$ and any $\boldsymbol{\xi}, \boldsymbol{\eta} \in \mathbb{R}^3$. Here $D_{\mathbf{F}}^2 W(\mathbf{F}).(\cdot, \cdot)$ is the second Fréchet derivative of W.

# Hill's stress in the linearization

As part of the tangent operator: $\left[\mathcal{D}R(\mathbf{U}_k^{n+1}, p_k^{n+1}, D_k^{n+1})(\Delta\mathbf{u}_k, \Delta p_k, \Delta D_k), (\delta\mathbf{U}, \delta p, \delta D)\right]$, we must compute the fourth-order elasticity tensor:

$$J^{4/3}\bar{\mathbb{C}}_{fibre}^{n+1} = 2\frac{\partial\bar{\mathbf{S}}_{fibre}^{n+1}}{\partial\bar{\mathbf{C}}^{n+1}} = 4\frac{\partial^2\Psi_{fibre}^{n+1}}{\partial\bar{\mathbf{C}}^{n+1}\partial\bar{\mathbf{C}}^{n+1}}$$

$$= \left\{ -\frac{2}{(\bar{\lambda}^{n+1})^4}\sigma_{Hill}(\bar{\lambda}^{n+1}, \bar{\bar{\varepsilon}}^{n+1}) + \frac{1}{(\bar{\lambda}^{n+1})^3}\frac{d\sigma_{Hill}(\bar{\lambda}^{n+1}, \bar{\bar{\varepsilon}}^{n+1})}{d\bar{\lambda}^{n+1}} \right\}\mathbb{M}_0,$$

where $\mathbb{M}_0 = \mathbf{a}_0 \otimes \mathbf{a}_0 \otimes \mathbf{a}_0 \otimes \mathbf{a}_0$. The ellipticity of W yields the following **necessary condition for polyconvexity:**

$$\frac{d\sigma_{Hill}(\bar{\lambda}^{n+1}, \bar{\bar{\varepsilon}}^{n+1})}{d\bar{\lambda}^{n+1}} \geq 0$$
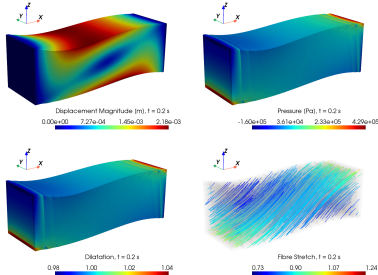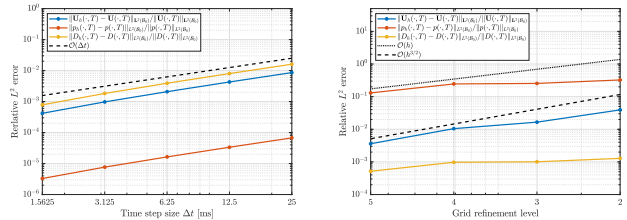
Existence of minimizers is not guaranteed
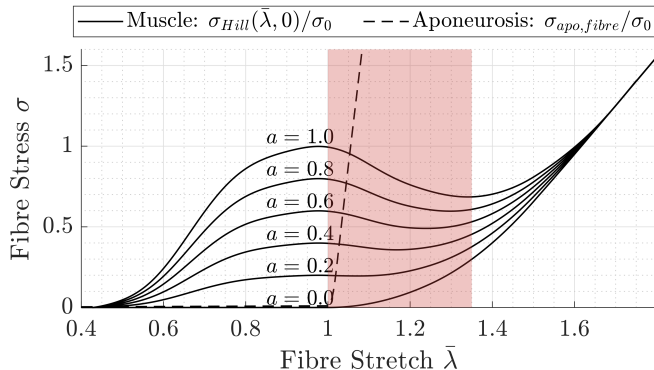
Figure 7: As activation increases, $\frac{d\sigma_A}{d\bar{\lambda}} < 0$ along the **descending limb** (shaded region). Hence, polyconvexity is **not** guaranteed. This may affect convergence.

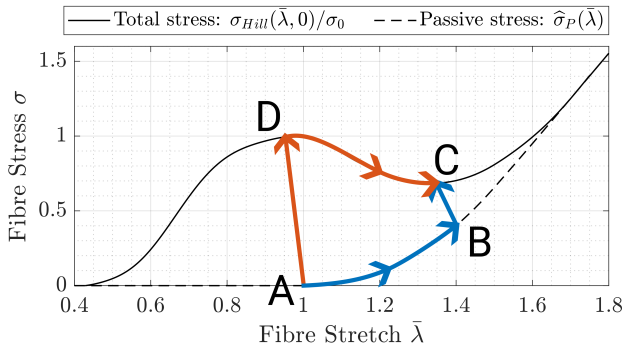# A convergence study on the nonlinear problem (§6.3)

Figure 8: Displacement **U**, pressure p, dilatation D, and fibre stretch λ at end state ($t = 0.2$ s).

Figure 9: Left: convergence in time of $\mathcal{O}(\Delta t)$ in all three variables. Right: convergence in space of $\mathcal{O}(h^{3/2})$ for **U**, and $\mathcal{O}(h)$ for p and D.

Two ways to reach the same active state (§6.4)

1. Path ABC (blue): passively lengthen the muscle, **then** activate. **Avoids descending limb**.
2. Path ADC (red): activate muscle, then lengthen.

Flexodeal: a New Finite-element Framework for Studying Musculoskeletal Dynamics

Flexodeal: a new framework to study MSK dynamics

- Open-source (v1.5.1): github.com/sfu-nml/flexodeal.

- **Fully dynamic** and quasi-static simulations supported.

- Computational domain can contain **muscle**, **tendon**, and **aponeurosis** tissue.

- User-defined boundary strain and activation profile can be provided with a table of data points.

- Quadrature-point data supported: intramuscular fat fraction, fibre directions, maximum isometric stress.

- Post-processed quantities such as **forces**, **energies**, **fibre stretch**, **fibre strain rate**, and **pennation** angle are available as CSV files.

- Minimal version of Flexodeal (useful for numerical analysis developments) implemented as **Flexodeal Lite**: github.com/sfu-nml/flexodeal-lite.

- Implementation based on deal.II (v9.3.1 or higher). Some elements are based on previous codes (Rahemi 2015, Dominguez 2020, Konno 2024, Tam 2024, and others).

Some MSK simulations
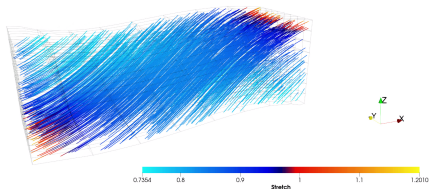
Figure 10: Isometric (fixed-end) contraction of a block of muscle tissue with fibres oriented at a 30° angle (cf. §6.3).
https://youtu.be/CCTiSV1Vl7o
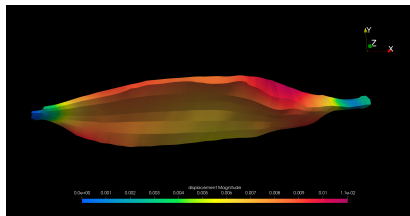
Figure 11: Cyclic contraction of a human medial gastrocnemius while running (cf. §6.6).
https://youtu.be/UtFPTZ7JW0w

Remark. The terms "fixed-end" and "isometric" are interchangeable but only when the computational domain is made of muscle tissue only (no tendon or aponeurosis; see Definition 6.1).

Gearing: a First-of-its-kind Computational Study

Gearing

- Gearing (also known as *architectural gearing ratio*), is defined as

$$\text{gearing} = \frac{\text{(avg) muscle velocity}}{\text{(avg) fibre velocity}}.$$

- Muscle-shape changes act as an automatic transmission system, allowing a pennate muscle to shift from a **high gear** during **rapid** contractions to **low gear** during **forceful** contractions (Azizi et al. 2008).

- It is a phenomenon that is typically studied *in vivo* or *in situ* at maximal activation (e.g. Randhawa et al. 2012, Holt et al. 2016) and computationally using models such as the McKibben pneumatic actuator (Azizi & Roberts 2013, Sleboda et al. 2024).
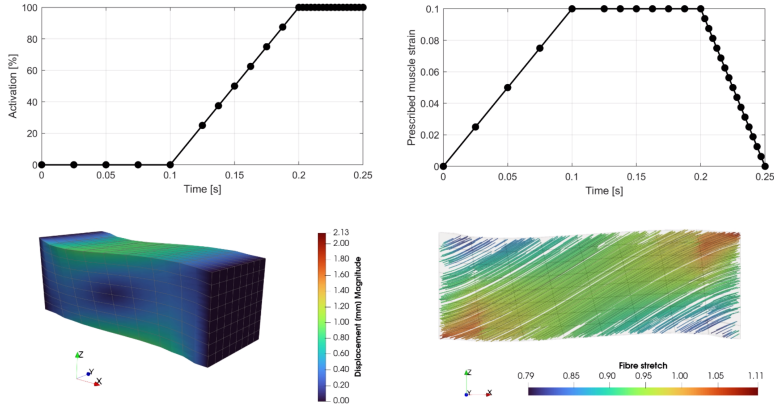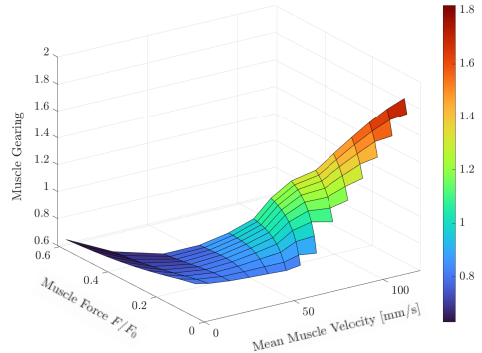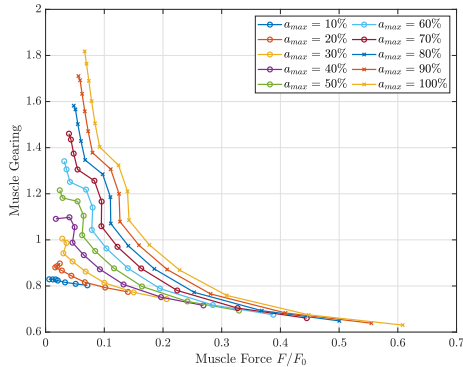
Gearing experiments (§7.2)

Figure 12: Blocks of muscle tissue with fibres oriented at a 26° angle are shortened at different speeds.
Video: https://youtu.be/Mlr9R1EWcol.

Variable gearing in a muscular structure (§7.3)

Figure 13: Our computations correctly capture the narrative that "gearing is higher when force is low and velocity is high" (Eng et al. 2018). Gearing magnitudes correlate well with the study by Holt et al. 2016.

Conclusions and Future work

Conclusions

This thesis covered the nonlinear elastodynamics of skeletal muscle tissue, combining:

- Tried-and-tested approaches from solid mechanics,
- Sound mathematical and numerical analysis principles,
- Well-recognized physiological results,
- Basic principles of software engineering.

Furthermore, the predicted inertial effects are in line with previous studies and demonstrate **the need for a dynamic simulation environment**.

Future work

Future work includes:

- Finite-element discretizations of 1D muscle models,
- Hu-Washizu formulations designed to include muscle force as a primary unknown,
- Develop a posteriori error estimators,
- Increase the efficiency of the computations (especially in terms of nonlinear solvers and parallel computing),
- Determination of experimental protocols that can validate Flexodeal simulations.

Resulting contributions

📄 **J. A. Almonacid, S. A. Dominguez-Rivera, R. N. Konno, N. Nigam, S. A. Ross, C. Tam & J. M. Wakeling.** A three-dimensional model of skeletal muscle tissues. *SIAM J. Appl. Math.* 84 (2024), no. 3, S538-S566.

📄 **I.-J. Chen, A. Latreche, S. A. Ross, J. A. Almonacid, T. J. M. Dick, E. E. Vereecke & J. M. Wakeling.** Effects of muscle mass on muscle force predictions in human movement. BioRxiv (2025). Submitted.

📄 **M. Pinto, J. M. Wakeling, J. A. Almonacid & A. Blaze-vich.** From muscle fibres to gears: How fibre rotation and shape change impact muscle function. BioRxiv (2025). Submitted.

📄 **J. A. Almonacid, N. Nigam & J. M. Wakeling.** On the stability of skeletal muscle. In preparation.
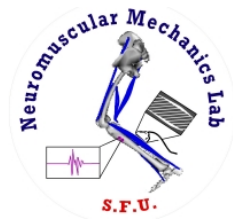
www.github.com/sfu-nml

www.github.com/javieralmonacid